Note on the time evolution sample for an adiabatic spherical case

A. Initial condition and parameter settings

Here we consider the adiabatic perturbation generated by the initial curvature perturbation ζ. As is described in Ref. [1], once the spatial profile of ζ is specified, the growing mode solution can be described up through the next-to-leading order of the long-wavelength approximation. We use the analytic expressions for the geometrical variables with the constant-mean-curvature and zero-shift gauge up through the next-to-leading order as the initial data for the sample code.

In this sample code, we consider the numerical domain given by $-L \leq X \leq L$, $0 \leq Y \leq L$ and $0 \leq Z \leq L$ with X, Y and Z being the reference Cartesian coordinates. The specific profile of the initial curvature perturbation is the same as in Ref. [2]:

$$\zeta = -\mu \exp\left(-\frac{1}{6}k^2R^2\right) W(R), \tag{1}$$

where $R^2 = X^2 + Y^2 + Z^2$ and the function $W(R)$ is given by [3]

$$W(R; R_{\rm W}, L) = \begin{cases} 1 & \text{for } 0 \leq R \leq R_{\rm W} \\ 1 - \frac{\left((R_{\rm W}-L)^6 - (L-R)^6\right)^6}{(R_{\rm W}-L)^{36}} & \text{for } R_{\rm W} \leq R \leq L \\ 0 & \text{for } L \leq R \end{cases} \tag{2}$$

with $R_{\rm W} = 0.8L$. The parameters k and μ are set as $k = 10/L$ and $\mu = 0.83$. The amplitude μ is slightly larger than the threshold value $\mu_{\rm th} \simeq 0.805$ for PBH formation reported in Ref. [2].

The background universe is assumed to be radiation-dominated, and the Hubble parameter at the initial time $H_{\rm i}$ is set to be $H_{\rm i} = 50/L$. The coordinate length L is covered by 40 grid points with grids on both ends. Since this sample code is just for demonstration, we do not seriously consider the constraint violations.

B. Non-Cartesian coordinate

In this sample code, we employ the non-Cartesian coordinate system (x, y, z) firstly implemented in Ref. [3]. The non-Cartesian coordinates x^i are related to the Cartesian coordinates X^i as follows:

$$X^i = x^i - \frac{\eta}{1+\eta}\frac{L}{\pi}\sin\left(\frac{\pi}{L}x^i\right). \tag{3}$$

This functional form is compatible with the boundary conditions adopted in this sample code (see Fig. 1. and Ref. [4]) and satisfies $x^i = 0$ at $X^i = 0$ and $x^i = L$ at $X^i = L$. At the origin, the infinitesimal interval in the Cartesian coordinate ΔX is covered by the non-Cartesian coordinate interval $\Delta x = (1+\eta)\Delta X$. Therefore the central part is enlarged in this non-Cartesian coordinate system. In this sample code, the value of η is set to 10.

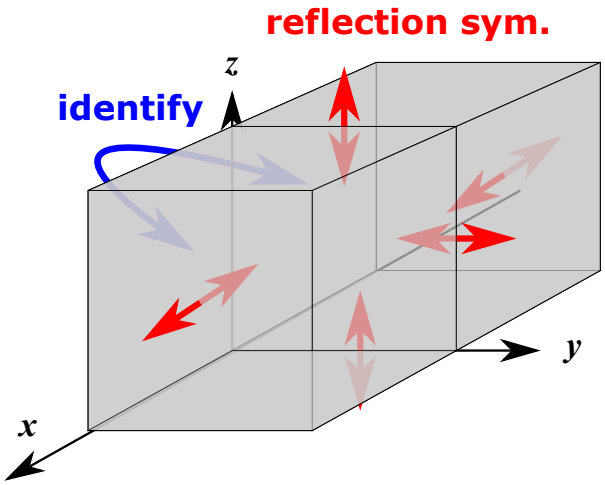

FIG. 1: The numerical region and boundary conditions.

C. Mesh refinement

On top of the non-Cartesian coordinate system, we implement fixed mesh refinement. We do not explain the details of our mesh refinement procedure but attach a simple schematic diagram showing our procedure (Fig. 2). In the sample code, 2 additional layers for the mesh refinement are introduced when the value of the lapse function at the origin reduces to 0.3 and 0.15. The region covered by one higher layer is the region covered by 10 grids in the lower layer. These parameters for the mesh refinement can be controlled by the parameter file `par_fmr.d`.

D. Results of the time evolution

In the default setting, the time evolution starts from the initial data described above. Then one finds PBH formation at around the coordinate time $t \simeq 61L$. It takes a very long time. We also attached the data file `ini_all.dat` which describes the system soon after the horizon formation. For instance, one can set the value of "*maximum step of the main loop*" in `par_ini.d` to 1 and set the value of the line indicated by "*0:no continue 1:continue*" to 1. When the numerical code is executed, first the data file `ini_all.dat`, in which 2 higher layers are already introduced, is loaded. Then the apparent horizon finder starts and a horizon will be found after some time (see Fig. 3). The time evolution starts after the apparent horizon finder. After just one step of the evolution, all the data will be restored into `out_all.dat`, and the calculation stops. The value of the lapse function on the x-y plane is depicted in Fig. 4.

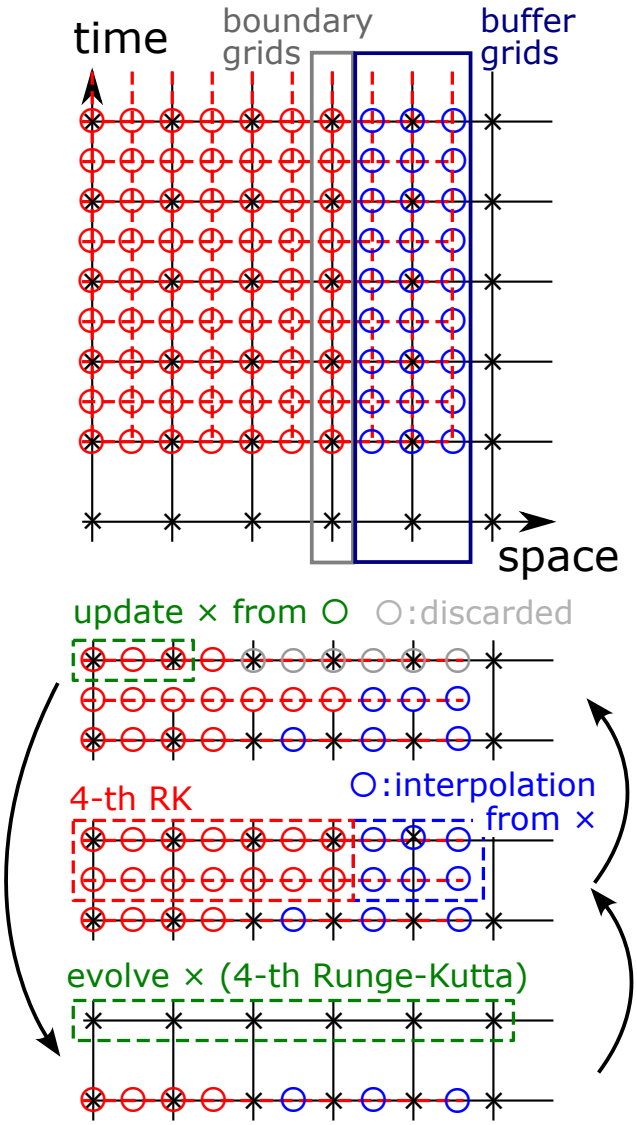

FIG. 2: The mesh refinement procedure.

E. Excision

When an apparent horizon is found, the excision prescription is introduced. We follow the procedure given in Ref. [5]. The region excised is a cubic region whose size can be controlled by the parameter "*excision grid*" in `par_ini.d`.

---

[1] T. Harada, C.-M. Yoo, T. Nakama, and Y. Koga, Phys. Rev. **D91**, 084057 (2015), arXiv:1503.03934, *Cosmological long-wavelength solutions and primordial black hole formation.*

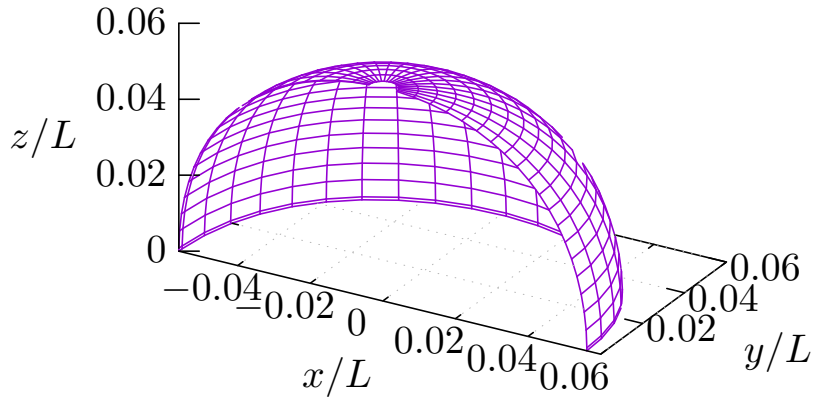

FIG. 3: Figure of Apparent horizon generated from `out_AHfig.dat`.

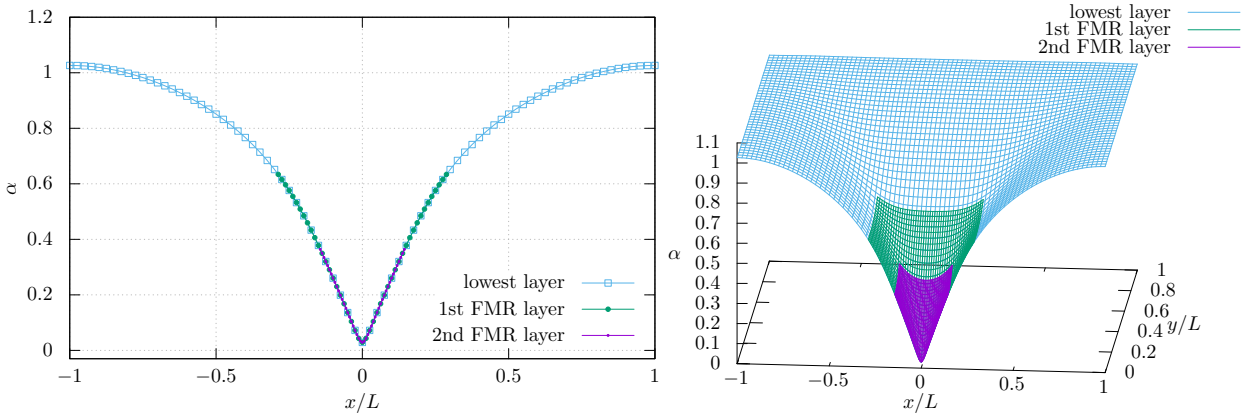

FIG. 4: Lapse function on the x-axis generated from 1st and 2nd columns in `out_xkl.dat`(left) and $x-y$ plane generated from 1st, 2nd and 3rd columns in `out_xyl.dat`(right).

[2] C.-M. Yoo, T. Harada, and H. Okawa, Phys. Rev. D **102**, 043526 (2020), arXiv:2004.01042, *Threshold of Primordial Black Hole Formation in Nonspherical Collapse*, [Erratum: Phys.Rev.D 107, 049901 (2023)].

[3] C.-M. Yoo, T. Ikeda, and H. Okawa, Class. Quant. Grav. **36**, 075004 (2019), arXiv:1811.00762, *Gravitational Collapse of a Massless Scalar Field in a Periodic Box.*

[4] C.-M. Yoo, Phys. Rev. D **110**, 043526 (2024), arXiv:2403.11147, *Primordial black hole formation from a nonspherical density profile with a misaligned deformation tensor.*

[5] M. Alcubierre and B. Bruegmann, Phys. Rev. D **63**, 104006 (2001), arXiv:gr-qc/0008067, *Simple excision of a black hole in (3+1)-numerical relativity.*